PCCP

Accepted Manuscript

ROYAL SOCIETY OF CHEMISTRY

www.rsc.org/pccp

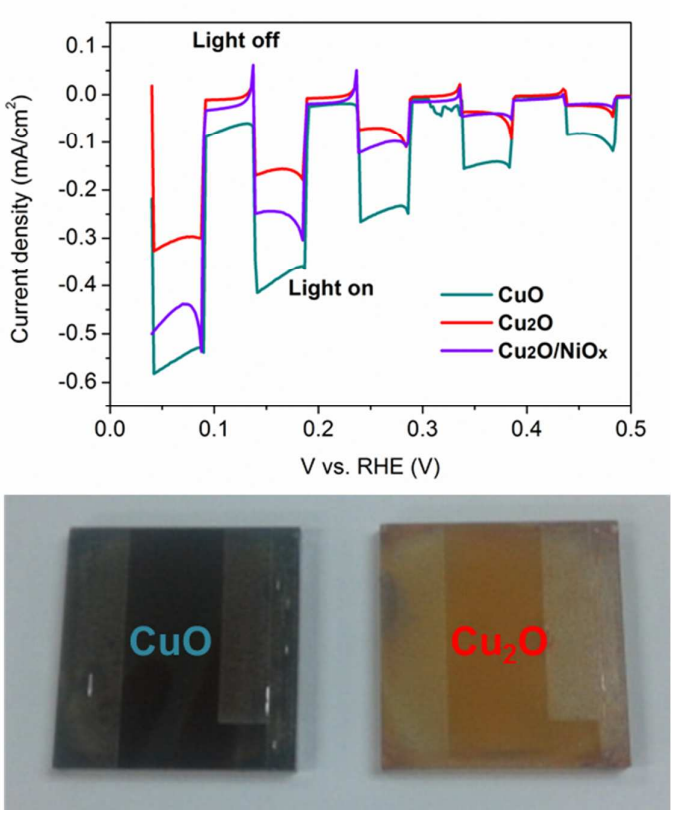

Cu_2O and CuO thin films deposited by spin-coating from a sol-gel process show promise for photocatalytic water splitting.

PCCP

RSCPublishing

ARTICLE

Sol-gel deposited Cu_2O and CuO thin films for photocatalytic water splitting

Cite this: DOI: 10.1039/xoxxoooooox

Yee-Fun Lim,*[a] Chin Sheng Chua,[a] Coryl Jing Jun Lee,[a] and Dongzhi Chi[a]

Received ooth January 2014,
Accepted ooth January 2014

DOI: 10.1039/xoxxoooooox

www.rsc.org/

Cu_2O and CuO are attractive photocatalytic materials for water splitting due to their Earth-abundance and low cost. In this paper, we report the deposition of Cu_2O and CuO thin films by a sol-gel spin-coating process. Sol-gel deposition has distinctive advantages such as low-cost solution processing, and uniform film formation over large areas with precise stoichiometry and thickness control. Pure phase Cu_2O and CuO films were obtained by thermal annealing at 500 °C in nitrogen and ambient air, respectively. The films were successfully incorporated as photocathodes in a photoelectrochemical (PEC) cell, achieving photocurrents of -0.28 mA cm^{-2} and -0.35 mA cm^{-2} (for Cu_2O and CuO, respectively) at 0.05 V vs. reversible hydrogen electrode (RHE). The Cu_2O photocurrent was enhanced to -0.47 mA cm^{-2} with the incorporation of a thin layer of NiO_x co-catalyst. Preliminary stability studies indicate that CuO may be more stable than Cu_2O as a photocathode for PEC water-splitting.

1. Introduction

One of the most attractive methods for storage of renewable solar energy is in the form of chemical bonds, through photocatalytic splitting of water into hydrogen and oxygen.[1] The criteria for choosing semiconductor photocatalysts to be employed in such photoelectrochemical cells (PECs) is quite similar to that for ideal photovoltaic materials, namely low band-gap, low toxicity, Earth-abundance, and low-cost.[2] In particular, cost is an important consideration, since PECs need to be cheap enough in order to compete with the alternative approach of wiring traditional photovoltaic panels to a commercial water-splitting electrolyser.[3]

A study by Wadia *et al.*,[2] based on considerations of cost, abundance and electricity potential, has identified both Cu_2O and CuO as promising materials for solar energy conversion. In addition, they are suitable as photocatalysts for hydrogen generation since the conduction band edges of both materials are more negative than the hydrogen evolution potential (-0.7 V and -0.2 V respectively for Cu_2O and CuO).[5,6] Cu_2O is a p-type semiconductor with a direct bandgap of 2 eV,[5] thus it is able to absorb visible light (in contrast with traditional photocatalysts like TiO_2 which absorb only in the UV) and has a theoretical photocurrent of 14.7 mA cm^{-2} under standard AM 1.5 irradiation.[5] Due to its above-mentioned favourable properties, it has been intensively studied as a hydrogen evolution photocatalyst by several research groups,[5,7-13] with experimental photocurrents above 7 mA cm^{-2} in optimized device configurations.[5] On the other hand, CuO is a p-type semiconductor with an indirect bandgap of 1.2-1.3 eV,[4,6] implying that it is theoretically capable of generating a much higher photocurrent of up to 35 mA cm^{-2}.[14] In comparison to Cu_2O, there are only very limited reports on the use of CuO as the active light-harvesting material for photocatalytic water splitting.[15-17] However, there have been several reports of CuO being applied as a co-catalyst for hydrogen evolution,[8,18-20] as the active material in solar cells,[21-25] and also in functional nanostructures and nanocomposites.[26-29]

Electrochemical deposition is the most common method utilized for the formation of Cu_2O thin film photocatalysts.[5,9-12] An attractive alternative that is much less commonly explored is deposition by spin-coating from sol-gel precursor solutions, followed by thermal annealing. Similar to electro-deposition, the sol-gel method has the advantage of low-cost processing from solution. In addition, sol-gel processing possesses some unique advantages, such as uniform and homogeneous film formation over large areas, and the possibility of precise stoichiometry and thickness control.[30,31] There are only a few reports of the deposition of Cu_2O thin films from a sol-gel process available in the literature.[32,33] Formation of the Cu_2O phase can be challenging since CuO is the stable phase that forms upon thermal annealing of the sol-gel precursor; Armelao *et al.* was able to obtain the Cu_2O phase only after annealing at 900 °C in a nitrogen-filled furnace tube for 5 hours.[32]

In this work, we report the deposition of pure-phase Cu_2O and CuO thin films by spin-coating from sol-gel precursor solutions. We will show that pure phase Cu_2O thin films can be obtained at a much lower annealing temperature of 500 °C inside a nitrogen glovebox. Additionally, the PEC performance of our sol-gel deposited Cu_2O and CuO thin films will be

presented to demonstrate their potential application for photocatalytic water-splitting. Finally, a thin layer of NiO_x co-catalyst was deposited to enhance the PEC photocurrent.[8] To the best of our knowledge, this is the first report of a Cu_2O thin film photocatalyst deposited by a sol-gel process.

2. Experimental

2.1 Synthesis of sol-gel precursor solutions

To prepare the copper oxide sol, 1.0 ml of ethanolamine (Sigma Aldrich) was added to 20 ml of 2-methoxyethanol (Sigma Aldrich) under vigorous stirring. Subsequently, 1.09 g of copper(II) acetate (Sigma Aldrich) was added, and dissolved completely after 15 minutes of stirring to form a deep blue solution with a concentration of 0.3 M. The role of the ethanolamine was to stabilize the solution and prevent formation of aggregates;[34,35] this was achieved by chelating with the copper acetate through O-Cu-O and O-Cu-N bonds.[35] Finally, 0.50 ml of poly(ethylene glycol) with an average molecular weight of 200 (Sigma Aldrich) was added to enhance film forming properties.[34] The solution was allowed to age for 2 days before use. All of the above steps were carried out at room temperature inside a nitrogen-filled glovebox.

The nickel oxide sol was prepared by dissolving 0.05 g of nickel(II) acetate tetrahydrate (Sigma Aldrich) in 10 ml of methanol (Tedia Company, Inc.) with 0.1 ml of ethanolamine. A light blue solution (0.02 M) was obtained, which was allowed to age for a day before use.

2.2 Thin film deposition

The copper oxide sol was spin-coated onto pre-pattermed fluorine-doped tin oxide (FTO) coated glass (Latech Scientific Supply, Singapore) and silicon substrates. Prior to spin-coating, the substrates were cleaned by sonication in isopropanol for 5 minutes, followed by oxygen plasma treatment for 2 minutes by a Trion Sirus reactive ion etcher. The sol-gel solution was pre-filtered with a 0.2 μm PVDF Whatman syringe filter before being dispensed onto the desired substrate. After spin-coating at the desired speed, the film was first dried on a hot-plate at 100 °C for 2 minutes, before being annealed at 350 °C for 5 minutes to convert the organic layer into oxide. This process was repeated to deposit multiple layers until the desired thickness was obtained. 10 cycles of spin-coating at 1500 rpm produced a film with a thickness of 300 nm, while a 600 nm thick film was obtained with 15 cycles of spin-coating at 1000 rpm.

In order to obtain the Cu_2O phase, the film was subjected to a final thermal annealing step at 500 °C on a hot-plate inside the nitrogen glovebox for 90 minutes. On the other hand, CuO thin films are obtained with a final anneal of 500 °C on a hot plate in ambient air for 10 minutes.

NiO_x co-catalyst was deposited by spin-coating the nickel oxide sol at 2000 rpm, followed by drying at 100 °C for 2 minutes and then annealing at 200 °C for 30 minutes. This is similar to the method previously reported by Lin *et al.*[8] The NiO_x thin film has a nominal thickness of 3-4 nm.

TiO_2 was deposited by atomic layer deposition (ALD) for encapsulation purposes on selected samples, using a Beneq TFS 200 ALD system with $TiCl_4$ and H_2O as precursors. A single reaction cycle comprised of the following sequence: $TiCl_4$ pulse (300 ms)/ purge (6 seconds)/ H_2O pulse (300 ms)/ purge (9 seconds). The reaction was allowed to proceed over 400 cycles at 200 °C, to produce a film that is about 20 nm thick.

2.3 Structural and optical characterization

X-ray diffraction (XRD) spectra were obtained with a Bruker D8 general area detector diffraction system (GADDS). X-ray photoelectron spectroscopy (XPS) was performed using a VG Thermo ESCALab 250i-XL X-ray photoelectron spectrometer with a monochromatic Al Kα (1486.6 eV) X-ray source. XPS data were charge corrected using the adventitious carbon C 1s peak at 285.0 eV as a reference. Thin film morphology was characterized by a field-emission scanning electron microscope (FE-SEM) ESM-9000. For UV-Vis absorbance studies, samples were measured with a Shimadzu 3101 UV-VIS-NIR spectrophotometer. Film thickness was measured using Woollam variable angle spectroscopic ellipsometry (WVASE32), and confirmed with cross-section SEM imaging.

2.4 Photoelectrochemical (PEC) testing

PEC measurements were performed in a 3-electrode configuration with a Ag/AgCl reference electrode, a Pt counter electrode, and the copper oxide thin film on FTO as the working electrode. The film was partially covered by black tape to define an active area of 1 cm^2. The electrodes were immersed inside a 0.1 M Na_2SO_4 aqueous electrolyte solution, with a pH of 5.84 as measured by a Hanna Instruments pH meter. A Metrohm Autolab PGSTAT101 potentiostat was used to supply the desired potential to the electrodes. The potentiostat was interfaced with NOVA 1.10 software for instrument control and automated data taking and recording. Current was measured in the dark, and also under illumination by an Oriel solar simulator with a 150 W Xenon arc lamp and AM 1.5 filter. The light intensity was maintained at 100 mW cm^{-2} as calibrated by a silicon photo-diode.

3. Results and discussion

The XRD spectra of the deposited copper oxide thin films on FTO are shown in Fig. 1. It can be seen that the film as deposited at 350 °C (Fig. 1(a)) exhibit the CuO phase, showing the distinct peaks for CuO crystal planes (-111) and (111) at $2\theta = 35.6°$ and $2\theta = 38.8°$ respectively (JCPDS# 05-0661). After annealing the film in nitrogen at 500 °C for just 30 minutes, it was possible to obtain a mixed phase of Cu_2O and CuO (Fig. 1(b)). Further annealing was necessary to eliminate the CuO phase; a pure-phase Cu_2O film was obtained after annealing in nitrogen at 500 °C for 90 minutes (Fig. 1(c)). In this film, the

peaks for the Cu_2O crystal planes (110), (111) and (200) at 2θ = 29.6°, 2θ = 36.5° and 2θ = 42.3° respectively (JCPDS# 05-0667) can clearly be identified, while CuO peaks are completely absent. On the other hand, the film annealed in ambient air at 500 °C for 10 minutes showed only crystal phases of CuO (Fig. 1(d)). These phase-pure Cu_2O and CuO films on FTO (corresponding to Fig. 1(c) and 1(d)) were the ones that were subsequently used for PEC testing. XRD spectra of copper oxide thin films deposited on Si were also obtained, so as to observe the copper oxide phase evolution without the SnO_2 peaks (Fig. S1 in the Supplementary Information).

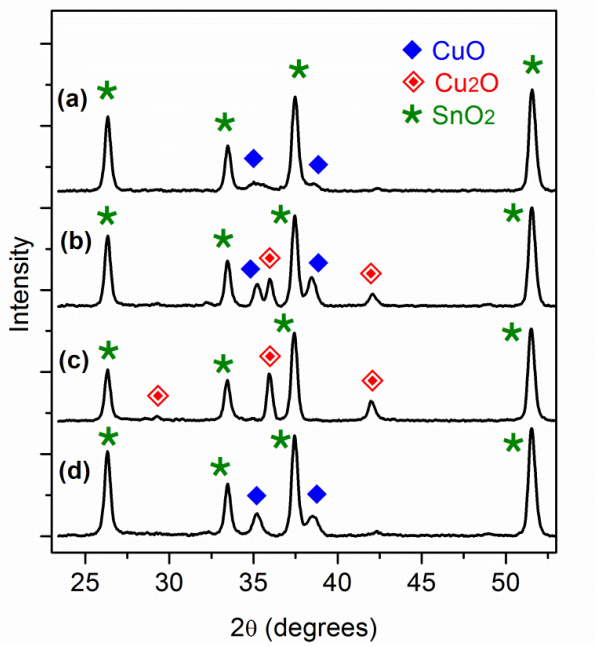

Fig. 1 XRD spectra of 300 nm thick copper oxide thin film deposited on FTO: (a) as deposited before final annealing; (b) annealed at 500 °C in nitrogen for 30 minutes; (c) annealed at 500 °C in nitrogen for 90 minutes; (d) annealed at 500 °C in ambient air for 10 minutes.

In order to investigate the growth of crystallite sizes with thermal annealing, values of the copper oxide crystallite sizes were calculated from the XRD spectra using the Scherrer equation.[36] CuO thin films as deposited at 350 °C have a crystallite size of 7.4 nm. The Cu_2O and CuO films, annealed at 500 °C for 90 minutes and 10 minutes respectively, exhibit crystallite sizes of 22.6 nm and 15.4 nm which are expectedly much larger than that of the as deposited film.

Since XRD may not be adequate in detecting minority or amorphous phase in the film, XPS spectra were also obtained to complement the XRD data. Using XPS, it is possible to distinguish between the Cu_2O and CuO phases by determining the binding energy of Cu $2p_{1/2}$ and $2p_{3/2}$, due to the relatively large difference of about 1 eV for the two copper oxide phases.[26,37,38] The XPS spectra of our thin films are plotted in Fig. 2, with indicated peak positions of the Cu $2p_{1/2}$ and $2p_{3/2}$ binding energies. These are consistent with literature values for Cu_2O and CuO.[26,37,38] Also consistent with literature is the presence of pronounced satellite peaks in the CuO spectrum, which are almost absent in the Cu_2O spectrum.

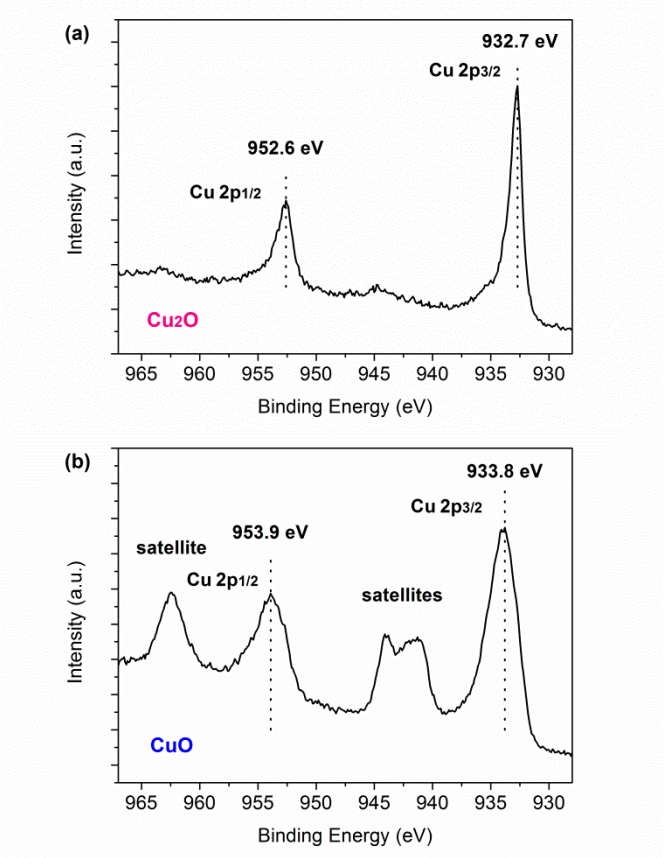

Fig. 2 XPS spectra of (a) Cu_2O; (b) CuO thin films. The peak positions indicated are that of the Cu $2p_{1/2}$ and $2p_{3/2}$ binding energies.

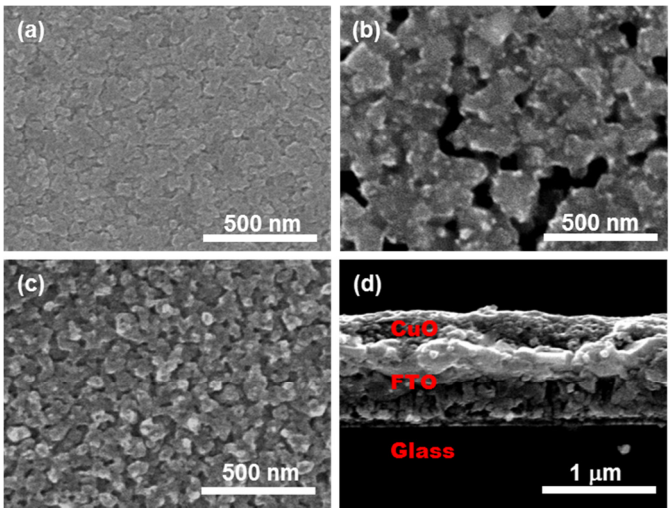

Fig. 3 SEM images of (a) as deposited CuO film; (b) Cu_2O film annealed at 500 °C in nitrogen; (c) CuO film annealed at 500 °C in ambient; (d) cross section of CuO film on top of FTO/glass.

Morphologies of the thin films are indicated in the SEM images in Fig. 3. The as deposited CuO film, as shown in Fig. 3(a), is relatively dense and crack-free with small crystallite size. Upon thermal annealing, porosity and crystallite size of the film increased, as seen from the images of annealed Cu_2O and CuO films in Fig. 3(b) and 3(c) respectively. The cross-section SEM images of the CuO film (Fig. 3(d) and Fig. S2 in the Supplementary Information) indicate a film thickness of approximately 300 nm.

The optical absorption properties of the FTO-supported films are shown in Fig. 4. Both Cu_2O and CuO absorb light across most of the UV and visible spectrum, as expected.

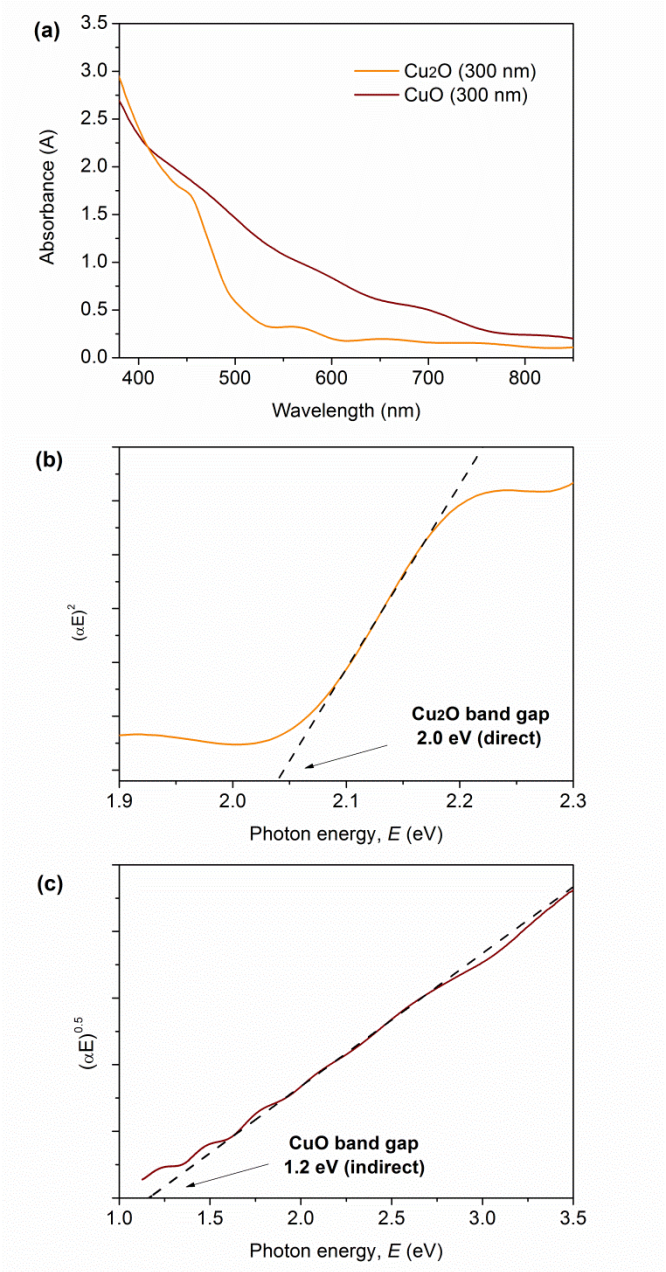

Fig. 4 (a) UV-Vis absorption spectra of 300 nm thick Cu_2O and CuO thin films deposited on FTO; (b) Tauc plot and band gap determination of Cu_2O thin film; (c) Tauc plot and band gap determination of CuO thin film.

From the absorbance data, the absorption coefficient α is calculated and used to generate Tauc plots for the band gap calculation.[39] For Cu_2O (direct gap) a plot of αE^2 is made against E (Fig. 4(b)), while for CuO (indirect gap) it is $\alpha E^{0.5}$ against E (Fig. 4(c)). From the Tauc plots, we obtain a band gap of 2.0 eV for Cu_2O and 1.2 eV for CuO, which is consistent with what has been reported in the literature.[4-6]

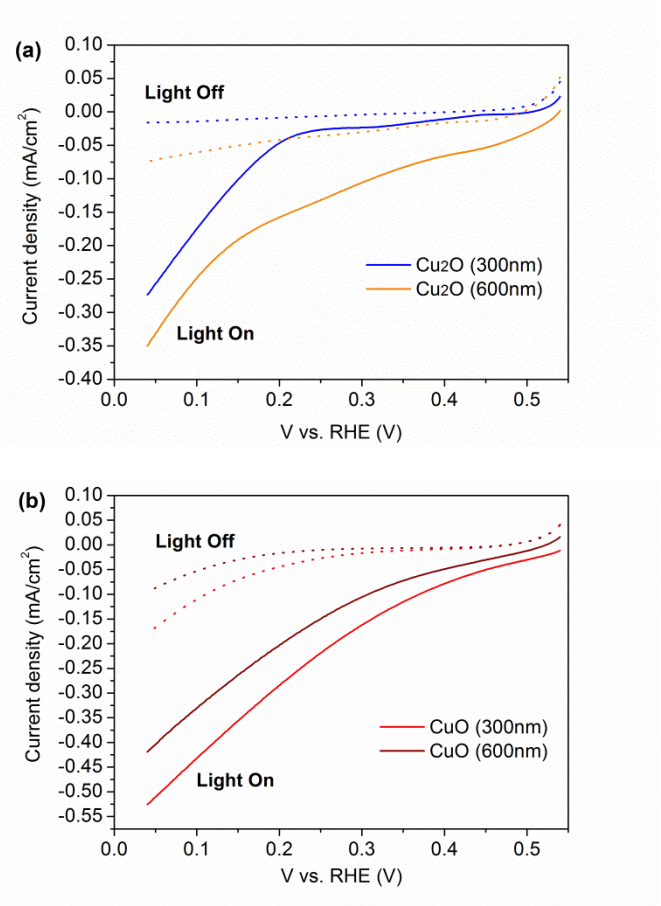

Fig. 5 PEC current-voltage measurements in the dark ("light off") and under AM 1.5 100 mW cm^{-2} illumination ("light on") for (a) Cu_2O; (b) CuO photocathodes.

PEC current-voltage curves are plotted in Fig. 5. The potential was originally measured with respect to a Ag/AgCl reference electrode, and then converted to the reversible hydrogen electrode (RHE) scale using the following equation:

$$E(RHE) = E(Ag/AgCl) + 0.197 + 0.059 \times pH \quad (1)$$

where *E(RHE)* is the potential on the RHE scale, *E(Ag/AgCl)* is the measured potential with respect to the Ag/AgCl reference electrode, and *pH* is the pH of the electrolyte which was measured to be 5.84.

The photocurrent is calculated by subtracting the current measured in the dark from the current measured under standard AM 1.5 100 mW cm^{-2} illumination. For Cu_2O photocathode (Fig. 5(a)), both the 300 nm film and the thicker 600 nm film

produced similar photocurrents of -0.26 mA cm^{-2} and -0.28 mA cm^{-2} respectively at 0.05 V vs. RHE. The performance of these films is somewhat inferior compared to that of the optimized Cu_2O photocathodes reported in the literature,[5,7-13] which typically have photocurrents above 1 mA cm^{-2} and even as high as 7 mA cm^{-2} in the best performing PEC.[5] However, it should be noted that the Cu_2O film is bare without any co-catalysts coated onto the surface, and our photocurrent of nearly -0.30 mA cm^{-2} is comparable to other reports for similarly unoptimized Cu_2O.[7,9]

Somewhat surprisingly, the much less studied CuO performed even better than Cu_2O; the 300 nm thick CuO film produced a photocurrent of -0.35 mA cm^{-2} at 0.05 V vs. RHE, while a similar photocurrent of -0.33 mA cm^{-2} was obtained by the thicker 600 nm film. In the literature, there are very few reports of water splitting based on CuO photocatalysts. Satsangi and Dass *et al.* reported that they have been able to achieve photocurrents on the order of 1-2 mA cm^{-2} with CuO; however, their use of non-standard light source and testing conditions makes comparison rather difficult.[15,16]

We find it interesting that the performance of CuO is better than Cu_2O, since a lot of research attention is focused on Cu_2O while CuO is almost completely neglected. A possible reason for the relative neglect of CuO may be due to its indirect band gap, thus it is perceived to have poor light absorption properties. However, it can be seen from Fig. 4(a) that for a similar film thickness, CuO has greater absorption than Cu_2O across virtually the entire visible spectrum. This may account for the higher photocurrent in CuO. Some researchers also have the perception that the conduction band position of CuO is not negative enough to drive the hydrogen evolution reaction.[8] In fact, the CuO conduction band edge was recently measured to be -0.6 V vs. normal hydrogen electrode (NHE) at pH 7 (similar to our electrolyte pH),[6] which corresponds to -0.2 V vs. RHE. Thus, the photocatalytic hydrogen evolution from water by CuO should be thermodynamically favourable. Our results are also consistent with previous work by Barreca *et al.*,[17] who reported higher rates of H_2 evolution from CuO photocatalysts as compared to Cu_2O photocatalysts.

In order to enhance the performance of our somewhat under-performing Cu_2O photocathode, a thin layer of NiO_x co-catalyst was deposited on top of the Cu_2O thin film. This strategy is similar to that previously reported by Lin *et al.*,[8] who showed that substantial enhancement of the Cu_2O photocurrent can be achieved with NiO_x co-catalyst. Our NiO_x film, deposited and annealed at 200 °C, is essentially amorphous with no peaks showing in the XRD spectrum (Fig. S3 in the Supplementary Information). Photocurrent performance of our Cu_2O and CuO photocathodes with the incorporation of NiO_x is shown in Fig. 6. For the 600 nm thick Cu_2O photocathode, the photocurrent increased from -0.28 mA cm^{-2} at 0.05 V vs. RHE to -0.47 mA cm^{-2} with the NiO_x co-catalyst, which is an enhancement of almost 70 %. No significant enhancement, however, was observed for the CuO photoelectrode, and the photocurrent remained about the same or decreased slightly with the incorporation of NiO_x.

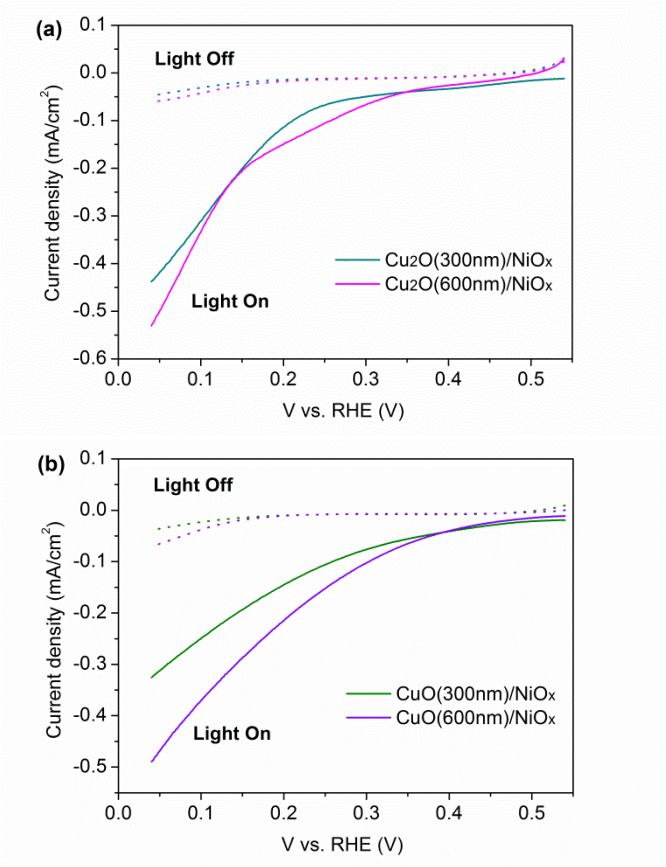

Fig. 6 PEC current-voltage measurements for (a) Cu_2O; (b) CuO photocathodes with the incorporation of NiO_x co-catalyst.

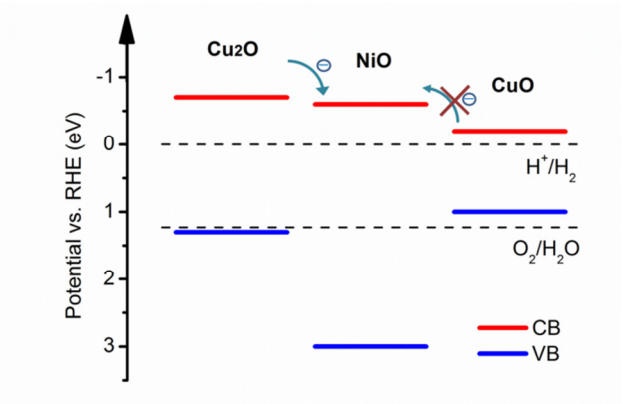

Fig. 7 Energy band positions vs. RHE for Cu_2O, NiO and CuO. Values are obtained from literature.[5,6,40]

An explanation for the above-mentioned effect can be found from the energy band positions for the conduction bands (CB) and valance bands (VB) of Cu_2O, NiO and CuO. The band position values, as obtained from literature,[5,6,40] are plotted in Fig. 7. It can be seen that electron transfer from Cu_2O to NiO is energetically favourable, but this is not the case for transfer

from CuO to NiO. The ability to efficiently transfer electrons to the hydrogen evolution sites in the NiO_x co-catalyst is crucial for enhancing the photocatalytic performance.[8,40] Hence, NiO_x can serve as an effective co-catalyst for Cu_2O but not CuO. It will be necessary to find another co-catalyst for CuO with suitable conduction band position.

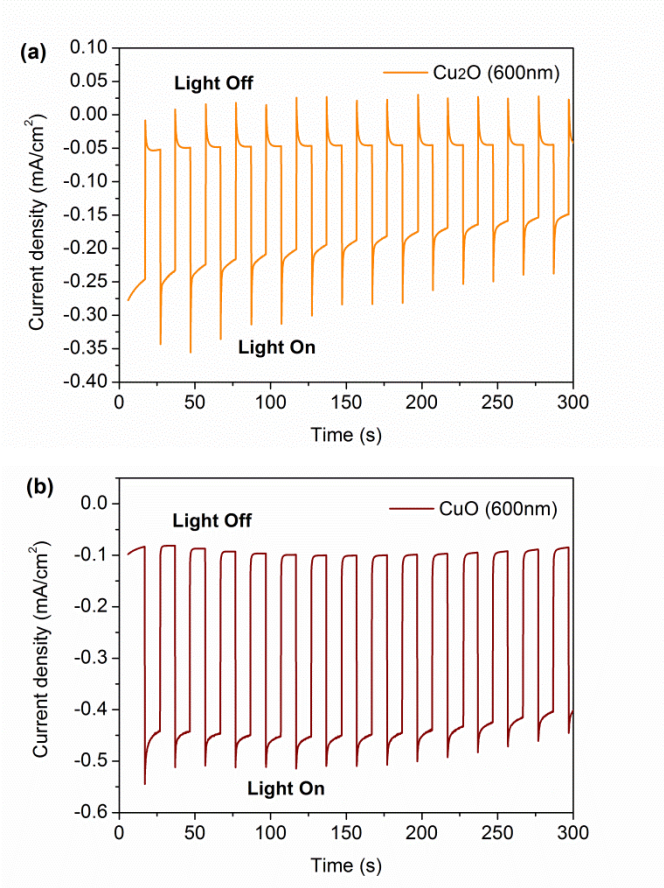

Fig. 8 Preliminary study of the photocurrent stability of the Cu_2O and CuO photocathodes over time.

A well-known issue of Cu_2O is that it is unstable in aqueous electrolytes.[5] To investigate this, a preliminary study of the photocurrent stability of the Cu_2O and CuO photocathodes was carried out by measuring the current over time at a constant potential of 0.05 V vs. RHE, and the results are plotted in Fig. 8. Over a timescale of 300 seconds, the degradation in Cu_2O photocurrent was quite significant, with about 60 % of initial photocurrent retained. Degradation was also observed in the CuO photocurrent, although the drop over the same timescale was smaller with about 90 % of initial photocurrent retained, which suggest that CuO may be more stable than Cu_2O.

The photostability of the NiO_x incorporated photocathodes have also been investigated (Fig. S4 in the Supplementary Information). The Cu_2O/NiO_x photocathode retained about 50 % of initial photocurrent after 300 seconds, while the CuO/NiO_x system retained about 85 % of initial photocurrent. Hence, the same trend was observed whereby the CuO is more stable than Cu_2O, although stability in the composite system has not improved. The ultra-thin layer of NiO_x (3-4 nm) is unlikely to be sufficient to encapsulate the copper oxide photocathodes.

A possible solution to the corrosion issue would be to encapsulate the photocathode with thin layers of ALD-deposited TiO_2 and ZnO.[5,10,12] Paracchino *et al.* encapulated their Cu_2O photocathode with an ALD-deposited stack of 5 × (4 nm ZnO/ 0.17 nm Al_2O_3)/ 11 nm TiO_2, which produced an electrode that retained 78 % of its initial photocurrent after 20 minutes of operation.[5] This is a significant improvement over the bare electrode, which showed negligible photocurrent after 20 minutes. Inspired by this approach, we have similarly encapsulated our Cu_2O photocathode with a layer of 20 nm thick TiO_2 that was deposited by ALD. After 300 seconds of operation, the photocurrent retained more than 90 % of its initial value (Fig. S5 in the Supplementary Information), which is a proof-of-concept demonstration that this approach can also work for our sol-gel deposited Cu_2O.

Another interesting observation in the current vs. time plots is the positive current spikes for the Cu_2O photocathode that occurred when the light was turned off. We believe a plausible origin of the current spikes may be related to transient effects from the corrosion of Cu_2O, which is known to occur according to the following reversible reaction:[5]

$$Cu_2O + H_2O + 2e^- \leftrightarrow 2Cu + 2OH^- \qquad (2)$$

Under illumination, a large number of electrons are photo-generated in the Cu_2O. According to Le Chatelier's principle, a system at equilibrium that is subjected to a change in concentration will readjust itself to counteract the change and establish a new equilibrium. Applied in this context, the excess photoelectrons would serve to drive the reaction towards the right and speed up the corrosion process. When the light is turned off, there is a sudden drop in the electron concentration, hence the reaction would be temporarily driven to the left (corresponding to a current in the opposite direction) until a new equilibrium is reached. This would explain the transient current spikes of the Cu_2O photocathode.

Conclusions

Pure-phase Cu_2O and CuO thin films have been successfully deposited from a sol-gel spin-coating process. An annealing temperature of 500 °C in nitrogen was sufficient to obtain the Cu_2O phase. When subjected to PEC testing under illumination, the bare Cu_2O and CuO photocathodes achieved photocurrents of -0.28 mA cm^{-2} and -0.35 mA cm^{-2} respectively at 0.05 V vs. RHE. Incorporation of NiO_x co-catalyst on top of the Cu_2O photocathode increased its photocurrent to -0.47 mA cm^{-2}, which is an enhancement of almost 70 %. This is the first report of a Cu_2O photocatalyst deposited by a sol-gel process, to the best of our knowledge. Preliminary stability studies indicate that although both CuO and Cu_2O suffer from corrosion and degradation of the photocurrent over time, the CuO photocathode may be more stable than Cu_2O. We hope these

results may motivate further research efforts in CuO as a water-splitting photocatalyst.

Acknowledgements

This work is supported by the Institute of Materials Research and Engineering (IMRE), A*STAR, through funding from core project IMRE/13-1C0102. We would also like to acknowledge technical support from the nano-fabrication, processing and characterization facility (SnFPC) at IMRE. In particular, we would like to thank Ms. June Ong for assistance with XPS measurements, and Dr. Yang Ren Bin for help with the ALD system.

Notes and references

[a] Institute of Materials Research and Engineering, A*STAR (Agency for Science, Technology and Research), Singapore 117602, Singapore.
E-mail: limyf@imre.a-star.edu.sg

Electronic Supplementary Information (ESI) available: additional XRD spectra, SEM images and photocurrent stability data. See DOI: 10.1039/b000000x/

1 N. S. Lewis and D. G. Nocera, *Proc. Natl. Acad. Sci. U. S. A.*, 2006, **103**, 15729.
2 C. Wadia, A. P. Alivisatos and D. M. Kammen, *Environ. Sci. Technol.* 2009, **43**, 2072.
3 P. Bornoz, F. F. Abdi, S. D. Tilley, B. Dam, R. van de Krol, M. Graetzel and K. Sivula, *J. Phys. Chem. C.* 2014, DOI: 10.1021/jp500441h.
4 F. P. Koffyberg and F. A. Benko, *J. Appl. Phys.* 1982, **53**, 1173.
5 A. Paracchino, V. Laporte, K. Sivula, M. Gratzel and E. Thimsen, *Nat. Mater.* 2011, **10**, 456.
6 M. Long, R. Beranek, W. Cai and H. Kisch, *Electrochim. Acta* 2008, **53**, 4621.
7 S. Yoon, M. Kim, I. S. Kim, J. H. Lim and B. Yoo, *J. Mater. Chem. A* 2014, **2**, 11621.
8 C. Y. Lin, Y. H. Lai, D. Mersch and E. Reisner, *Chem. Sci.* 2012, **3**, 3482.
9 Z. Zhang and P. Wang, *J. Mater. Chem.* 2012, **22**, 2456.
10 A. Paracchino, N. Mathews, T. Hisatomi, M. Stefik, S. D. Tilley and M. Gratzel, *Energy Environ. Sci.* 2012, **5**, 8673.
11 Z. Zhang, R. Dua, L. Zhang, H. Zhu, H. Zhang and P. Wang, *ACS Nano*, 2013, **7**, 1709.
12 C. G. Morales-Guio, S. D. Tilley, H. Vrubel, M. Gratzel and X. Hu, *Nat. Commun.*, 2014, **5**, 3059.
13 A. Martinez-Garcia, V. K. Vendra, S. Sunkara, P. Haldankar, J. Jasinski and M. K. Sunkara, *J. Mater. Chem. A*, 2013, **1**, 15235.
14 C. Liu, N. P. Dasgupta and P. Yang, *Chem. Mater.*, 2014, **26**, 415.
15 Y. S. Chaudhary, A. Agrawal, R. Shrivastav, V. R. Satsangi and S. Dass, *Int. J. Hydrogen Energy*, 2004, **29**, 131.
16 D. Chauhan, V. R. Satsangi, S. Dass and R. Shrivastav, *Bull. Mater. Sci.*, 2006, **29**, 709.
17 D. Barreca, P. Fornasiero, A. Gasparotto, V. Gombac, C. Maccato, T. Montini and E. Tondello, *ChemSusChem*, 2009, **2**, 230.
18 Z. Jin, X. Zhang, Y. Li, S. Li, G. Lu, *Catal. Commun.* 2007, **8**, 1267.
19 Z. Liu, H. Bai, S. Xu, D. D. Sun, *Int. J. Hydrogen Energy*, 2011, **36**, 13473.
20 Y. H. Pai and S. Y. Fang, *J. Power Sources*, 2013, **230**, 321.
21 P. Wang, X. Zhao and B. Li, *Opt. Express*, 2011, **19**, 11271.
22 F. Gao, X. J. Liu, J. S. Zhang, M. Z. Song and N. Li, *J. Appl. Phys.* 2012, **111**, 084507.
23 S. Chandrasekaran, *Sol. Energy Mater. Sol. Cells*, 2013, **109**, 220.
24 Y. F. Lim, J. J. Choi and T. Hanrath, *J. Nanomater.* 2012, 393160.
25 T. Dimopoulos, A. Peic, P. Mullner, M. Neuschitzer, R. Resel, S. Abermann, M. Postl, E. J. W. List, S. Yakunin, W. Heiss and H. Bruckl, *J. Renewable Sustainable Energy* 2013, **5**, 011205.
26 D. Barreca, A. Gasparotto, C. Maccato, E. Tondello, O. I. Lebedev and G. V. Tendeloo, *Cryst. Growth Des.* 2009, **9**, 2470.
27 D. Barreca, G. Carraro, E. Comini, A. Gasparotto, C. Maccato, C. Sada, G. Sberveglieri and E. Tondello, *J. Phys. Chem. C* 2011, **115**, 10510.
28 D. Barreca, G. Carraro, A. Gasparotto, C. Maccato, O. I. Lebedev, A. Parfenova, S. Turner, E. Tondello and G. V. Tendeloo, *Langmuir* 2011, **27**, 6409.
29 D. Barreca, G. Carraro, A. Gasparotto, C. Maccato, M. Cruz-Yusta, J. L. Gomez-Camer, J. Morales, C. Sada and L. Sanchez, *ACS Appl. Mater. Interfaces* 2012, **4**, 3610.
30 L. L. Hench and J. K. West, *Chem. Rev.* 1990, **90**, 33.
31 Q. X. Jia, T. M. McCleskey, A. K. Burrell, Y. Lin, G. E. Collis, H. Wang, A. D. Q. Li and S. R. Foltyn, *Nat. Mater.* 2004, **3**, 529.
32 L. Armelao, D. Barreca, M. Bertapelle, G. Bottaro, C. Sada and E. Tondello, *Thin Solid Films*, 2003, **442**, 48.
33 S. C. Ray, *Sol. Energy Mater. Sol. Cells*, 2001, **68**, 307.
34 A. Y. Oral, E. Mensur, M. H. Aslan and E. Basaran, *Mat. Chem. Phys.* 2004, **83**, 140.
35 Y. Takahashi, A. Ohsugi, T. Arafuka, T. Ohya, T. Ban and Y. Ohya, *J. Sol-Gel Sci. Technol.* 2000, **17,** 227.
36 A. L. Patterson, *Phys. Rev.* 1939, **56**, 978.
37 S. Poulston, P. M. Parlett, P. Stone and M. Bowker, *Surf. Interface Anal.* 1996, **24**, 811.
38 J. P. Espinos, J. Morales, A. Barranco, A. Caballero, J. P. Holgado and A. R. Gonzalez-Elipe, *J. Phys. Chem. B* 2002, **106**, 6921.
39 O. Stenzel, *The Physics of Thin Film Optical Spectra*, Springer-Verlag, Berlin, Germany 2005.
40 A. Kudo and Y. Miseki, *Chem. Soc. Rev.* 2009, **38**, 253.